Journal of Materials Chemistry C

Accepted Manuscript

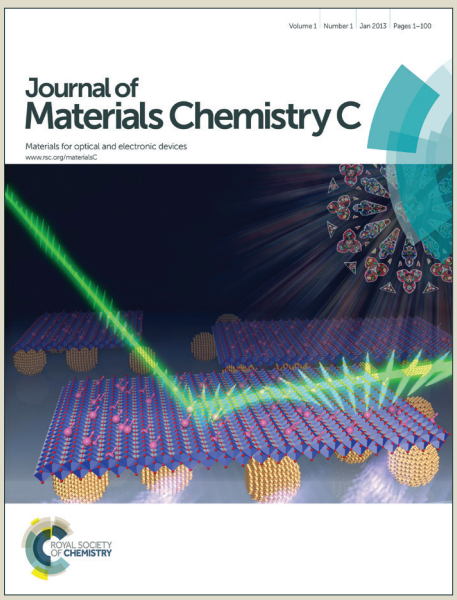

ROYAL SOCIETY OF CHEMISTRY

www.rsc.org/materialsC

Journal of Materials Chemistry C

RSCPublishing

ARTICLE

Cite this: DOI: 10.1039/x0xx00000x

Intense Ultraviolet Upconversion in Water Dispersible $SrF_2:Tm^{3+}$, Yb^{3+} Nanoparticles: Effect of the Environment on Light Emissions

Received ooth January 2012,
Accepted ooth January 2012

DOI: 10.1039/x0xx00000x

www.rsc.org/

M. Quintanilla,[a] I. X. Cantarelli,[b] M. Pedroni,[b] A. Speghini*,[b] and F. Vetrone*,[a, c]

Water dispersible $SrF_2:Tm^{3+}$, Yb^{3+} upconverting nanoparticles (9 nm diameter) have been synthesized to elucidate their potential as ultraviolet emitters. High intensity upconversion ultraviolet emission bands centered at 350 and 360 nm were detected following excitation at in the near-infrared 980 nm for H_2O and D_2O colloidal dispersions of the upconverting nanoparticles, corresponding to transitions from the $^1I_6$ and $^1D_2$ energy levels of thulium (Tm^{3+}) ions. Both emission intensities were strongly dependent on the temperature and the H_2O/D_2O molar ratio in the media, two important criteria that define the different environments in which the nanoparticles can be applied. Since the variations observed were different for each emitting level, the relevance of each band is discussed in relation to these two criteria.

Introduction

Near ultraviolet (UV) light is a key excitation frequency for several applications in biomedicine.[1] For instance, most of the fluorescent materials widely used for biomedical imaging and FRET-based biosensors, including commonly used organic dyes and quantum dots, have a strong absorption cross-section in the UV region, and thus can work efficiently in this range. Moreover, UV light has been proposed as an alternative strategy to control, both in time and space, the killing of cancer cells by activating either therapeutic antibodies modified to be light-sensitive[2] or photosensitizing drugs previously injected in the tumor.[3, 4] Also, UV light is absorbed by semiconductors such as ZnO or TiO_2 that are found to be useful in photocatalysis for hydrolysis and as bactericide agents for the detoxification of waste water and even for cancer therapy.[5-7]

In general, all these applications are carried out under direct UV excitation. However, for biomedical applications that take place in physiological environments, direct UV excitation becomes a problem since it is strongly absorbed by biological tissues (e.g. skin, blood) and therefore a very limited penetration depth of the excitation light is achieved.[8] For these reasons, UV-sensitive compounds are a viable option only if they can be placed close to the skin surface, as is the case of photodynamic skin cancer therapy, or when the use of invasive techniques is possible, including the use of optical fibers to guide the light to the chosen site.

On the other hand, biological and water-based media are highly transparent to near-infrared (NIR) radiation in the so-called "biological window" for wavelengths in the 750-1000 nm range.[8, 9] In this regard, a promising option to broaden the field in which UV-sensitive compounds can be applied is provided by certain lanthanide (Ln^{3+})-doped materials that are able to transform NIR light into higher energy photons, such as visible or UV light via a process known as upconversion.[10, 11] Therefore, with upconverting nanoparticles (UCNPs) it would be possible to use NIR excitation, and then transform the light into UV directly inside the biological or aqueous environment, improving thus the penetration depth allowed for the technique.

UCNPs are generally based on highly transparent materials, where the dopant Ln^{3+} ions are the active centers that provide the needed energy levels for multiple photon addition to occur.[12] The position and characteristics of these energy levels allow the promotion of electrons in subsequent steps, first from the ground state to an excited state, and then from one excited state to a higher energy one. Consequently, upconversion is a multistep process in which the energy of the final emitted photon is obtained by adding the energy of several excitation photons.

A great deal of work has been carried out over the last several years to obtain UCNPs that show strong upconversion emissions, no small feat considering the multi-step nature of the upconversion process where each subsequent step should be less probable.[13, 14] Moreover, an even bigger challenge has been to obtain water dispersible UCNPs with strong UV emission, especially for targeting the applications mentioned above.[15, 16] Upconversion emission of UCNPs dispersed in aqueous environments is usually strongly quenched due to relevant non-radiative relaxation processes, resulting from the high phonon energy cut-off of the water molecule (around 3600 cm^{-1}) that induces fast multiphonon relaxation. In fact, due to the high surface to volume ratio for nanosized systems, the number of Ln^{3+} ions on the particle surface is relatively high and therefore their luminescence could be easily quenched by the

solvent. Indeed, this adds an additional hurdle to overcome thereby rendering it difficult to obtain strong UV-emitting materials with sizes below 10 nm. In a previous work by Qiu et al, water dispersible YF_3:Tm^{3+},Yb^{3+} rhombic nanoparticles of 14 nm side and 2.5 nm thickness were reported.[15] However, sub-10 nm UCNPs with strong upconversion in the UV region still remains elusive.

To guarantee a good UV signal from water dispersible UCNPs, the host needs to fulfil certain characteristics, such as having a high-energy absorption edge, to prevent it from absorbing UV light. Additionally, the vibrational energies (phonons) of the crystalline host should be as low as possible, to minimize non-radiative relaxations. In that regard, several fluorides including CaF_2, SrF_2 and BaF_2 are widely known transparent materials in UV optics applications.[17-20] Also, they are particularly suitable hosts since they have low reported cut-off phonon energies (321 cm^{-1}, 285 cm^{-1} and 241 cm^{-1}, respectively)[21] in the same order of magnitude or at even lower energies than the cut-off phonons reported for widely used upconversion hosts such as $NaYF_4$ (360 cm^{-1}) or YF_3 (514 cm^{-1}).[22, 23] Indeed, Tm^{3+}/Yb^{3+} co-doped CaF_2 and SrF_2 nanoparticles have been demonstrated to show better qualities than cubic-$NaYF_4$ to obtain 800 nm upconversion after 980 nm excitation, which constitutes a promising characteristic since UV generation in Tm^{3+},Yb^{3+}-doped materials is based on this upconversion process as an intermediate step.[24]

In the present investigation we propose water dispersible SrF_2-based UCNPs (9 nm diameter) doped with Tm^{3+} and Yb^{3+} ions as efficient nanomaterials to obtain high intensity UV emission through upconversion processes. Since the upconverted emissions are known to be dependent on the temperature and on the presence of water on the nanoparticle surface, the emission intensity is discussed in these terms to consider the applicability of the proposed nanoparticles.

Experimental Techniques

Synthetic procedures

Ln^{3+}-doped SrF_2 UCNPs were synthesized by a hydrothermal method developed by our group.[24] Briefly, stoichiometric amounts of the metal chlorides $SrCl_2{\cdot}2H_2O$, $YbCl_3{\cdot}6H_2O$ and $TmCl_3{\cdot}6H_2O$ (Aldrich 99.9 %) were dissolved in 7 mL of deionized water (total metal content equal to 3.5 mmol) and Sr:Yb:Tm = 77.8:22:0.2 molar ratios. To this solution, 25 mL of sodium citrate (0.8 M) and 3.0 mL of NH_4F (3.5 M, Aldrich, 99.9 %) solutions were added. The resultant clear solution was heated in a 50 mL stainless steel Teflon lined digestion pressure vessel (DAB-2, Berghof) at 190 °C for 6 h. After washing with acetone and drying at room temperature, the obtained UCNPs (25 g/L) were directly dispersed in deionized water and filtered with a 450 nm cut off filter. The dispersions remained stable for more than two months.

Characterization Methods

Dynamic light scattering (DLS) and zeta potential measurements of the SrF_2:Tm^{3+}, Yb^{3+} UCNPs (1.25 g/L) were carried out in filtered deionized water solutions using a Malvern Zetasizer Nano ZS90 operating with a HeNe laser at 633 nm. The size distribution and the morphology of the obtained SrF_2:Tm^{3+},Yb^{3+} UCNPs were evaluated using high-resolution transmission electron microscopy images (HRTEM - Philips CM200). For the characterization of the upconverted luminescence, a 980 nm cw fiber-coupled laser diode (Thorlabs) with a maximum power of 330 mW was used (the diameter of the spot was 0.4 mm). Coated fused silica lenses were used to focus the excitation light on the sample and the resultant upconversion emission was collected in a 90° configuration. The upconverted light was then transferred to a spectrophotometer (Avaspec - 2048L - USB2) through an optical fiber. All the upconversion emission spectra obtained were subsequently corrected using the response curve of the luminescence set-up (lenses, fiber and detector), which was calibrated using an Ocean Optics halogen tungsten lamp as a reference. The upconversion luminescence studies were performed using highly transparent quartz cuvettes (Hellma) to avoid any UV absorption. Finally, the thermal measurements were carried out using a thermometric stage (Avantes qpod2e) that guarantees a homogeneous thermal distribution across the cuvettes used.

Results and discussion

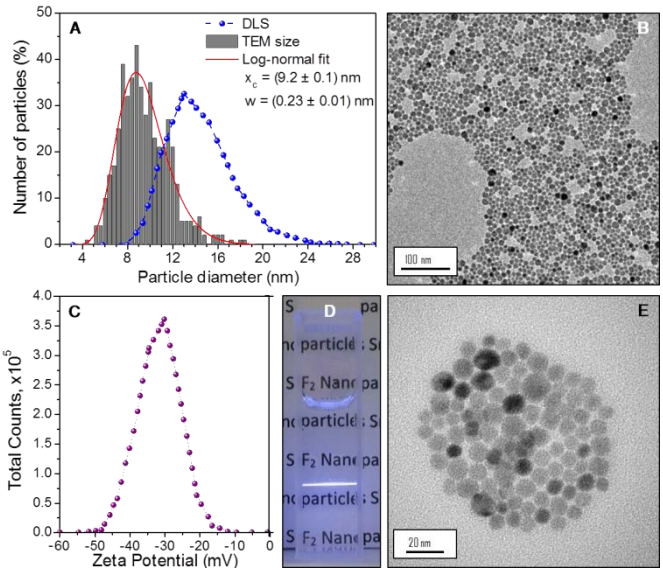

Figure 1. (A) Size distribution of the synthesized UCNPs obtained from TEM images and hydrodynamic diameter obtained from DLS measurements. (B) and (E) TEMs images with different magnifications showing the spherical morphology and homogeneity of the particles. (C) Zeta potential obtained for nanoparticles in deionized water and (D) picture of the sample in D_2O excited at 980 nm.

The synthesized SrF_2:Tm^{3+},Yb^{3+} UCNPs were single phase, as demonstrated by X-ray analysis[24] and the TEM images (shown in Figure 1B, E) demonstrate that they have a spherical shape with an average diameter of 9 nm, determined after measuring several hundreds of UCNPs. The average hydrodynamic size of the UCNPs was measured on a colloidal dispersion in deionized water (see Figure 1A) and a value 16 ± 2.5 nm was found, with a polydispersity index (PDI) of 0.23, confirming the absence of aggregation. The Z-potential in deionized water was determined to be -31.5 ± 5.8 mV (Figure 1C), demonstrating a very good colloidal stability. We have observed that the nanoparticles dispersed in water are stable for a period of up to two months without any noticeable precipitation or flocculation. Moreover, this is in line with work of Singh et al.,[25]

which reported that the stability constant of the Ca^{2+}-cit^{3-} complex is very high, on the order of 7.0 x 10^4, it is thus reasonable to assume that the bonding between the Ca^{2+} ions on the surface of the nanoparticles and the citrate ions is very strong. Therefore, it would be quite difficult to lose citrate ions from the surface of the nanoparticles under ambient conditions. A picture of the sample is shown in Figure 1D to show the high transparency of the dispersion.

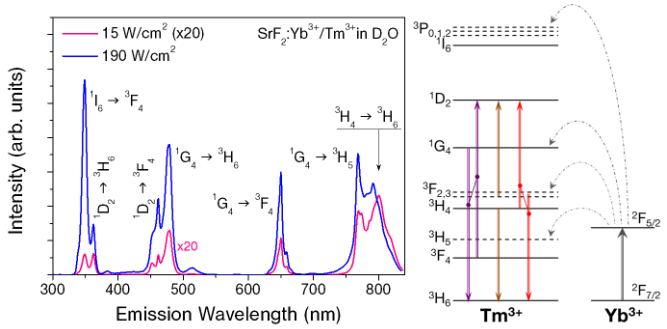

Figure 2. Left: Emission spectrum from the near UV to the NIR of SrF_2:Tm^{3+}, Yb^{3+} UCNPs at room temperature in D_2O (980 nm). Right: A partial energy level diagram of the system Tm^{3+}/Yb^{3+} showing Yb^{3+} to Tm^{3+} energy transfer (black dashed curved arrows) and cross-relaxation Tm^{3+} to Tm^{3+} processes (solid colored lines).

The Tm^{3+}/Yb^{3+} upconversion mechanisms are described in Figure 2 (right side). Briefly, after illumination at 980 nm, the Yb^{3+} ions are excited to their $^2F_{5/2}$ excited state. Then, since the energy of this state is very close to the energy associated with the transition between the ground state of Tm^{3+} ions ($^3H_6$) and the $^3H_5$ excited state, the energy transfer process $^2F_{5/2}$ (Yb^{3+}) + $^3H_6$ (Tm^{3+}) → $^2F_{7/2}$ (Yb^{3+}) + $^3H_5$ (Tm^{3+}) takes place, populating the $^3H_5$ excited state of the Tm^{3+} ions. Due to the small energy gap between the $^3H_5$ - $^3F_4$ states, the $^3H_5$ level is quickly depopulated with a multiphonon relaxation process that populates the lower lying $^3F_4$ level. At that point, when a second Yb^{3+} ion absorbs a 980 nm photon and is excited to the $^2F_{5/2}$ state, a second energy transfer from Yb^{3+} to Tm^{3+} can occur, $^2F_{5/2}$ (Yb^{3+}) + $^3F_4$ (Tm^{3+}) → $^2F_{7/2}$ (Yb^{3+}) + $^3F_{2,3}$ (Tm^{3+}), populating the higher energy states $^3F_2$ and $^3F_3$ (summarized as $^3F_{2,3}$ from now on due to their very close energies). The $^3F_{2,3}$ state of Tm^{3+} is mostly depopulated following a non-radiative route that populates the lower lying state, $^3H_4$. Finally, in a third energy transfer process from Yb^{3+} to Tm^{3+} ions, it is possible to populate the higher $^1G_4$ state following the mechanism $^2F_{5/2}$ (Yb^{3+}) + $^3H_4$ (Tm^{3+}) → $^2F_{7/2}$ (Yb^{3+}) + $^1G_4$ (Tm^{3+}).

Figure 2 (left side) shows the recorded upconversion emission spectrum of a colloidal dispersion of SrF_2:Tm^{3+}, Yb^{3+} UCNPs in D_2O after excitation at 980 nm as well as the corresponding band assignments for two excitation powers. The spectrum shows strong emissions in the NIR, red and blue ranges related to the relaxation of the $^3H_4$ and $^1G_4$ levels, which are populated as described above. It is highly remarkable that a strong emission band in the UV, with two features around 350 and 370 nm, is observed. These bands can be assigned to the radiative transitions of the $^1D_2$ and $^1I_6$ levels, (see the scheme on the right of Figure 2). The upconversion route that populates $^1D_2$ state is often described as a combination of several energy transfer processes that can be grouped in two main mechanisms. On one side, an additional Yb^{3+} to Tm^{3+} energy transfer process can take place, $^2F_{5/2}$ (Yb^{3+}) + $^1G_4$ (Tm^{3+}) → $^2F_{7/2}$ (Yb^{3+}) + $^1D_2$ (Tm^{3+}). Nevertheless, due to the strong non-resonant character of this process, Tm^{3+} to Tm^{3+} cross-relaxation processes, such as $^1G_4$ → $^3H_6$:$^3F_4$ → $^1D_2$ (solid purple line); $^3H_4$ → $^3H_6$:$^3F_{2,3}$ → $^1D_2$ (solid brown line) or $^3F_{2,3}$ → $^3H_6$:$^3H_4$ → $^1D_2$ (solid red line), must be considered as well.[27, 28] These cross-relaxations are all resonant therefore their contributions are significant and cannot be neglected. Finally, the population of $^1I_6$ takes place after a fifth energy transfer process from excited Yb^{3+} ions in the vicinity. In this case the acceptor states, $^3P_{0,1,2}$ account for a higher energy than $^1I_6$ but are energetically close to each other in a way that makes the multiphonon relaxation down to $^1I_6$ a very probable relaxation route. It must be noted that for lower excitation powers, UV emission becomes weaker and most of the upconverted electrons generate 800 nm light. The bandshape of the emission at this wavelength thus appears different at different powers, since it is the superposition of two different contributions: one related to $^3H_4$ → $^3H_6$ transition, stronger at lower powers, and another one from $^1G_4$ → $^3H_5$, stronger at higher powers.[26]

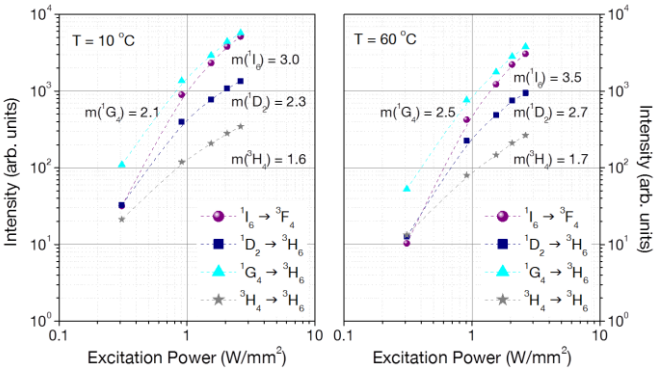

Figure 3. Power dependence of the SrF_2:Tm^{3+},Yb^{3+} emission bands at 10 °C (A) and 60 °C (B). The dashed lines have been added to guide eye. The values *m* correspond to the slope of a linear fit of the data recorded at lower powers.

A further insight into the upconversion mechanisms is commonly provided by the dependency of the emission intensity on the excitation power (Figure 3). It is known that the slope relating these two magnitudes in a log-log plot, *m*, is directly linked to the minimum number of photons required to populate each emitting level, *n*. Nevertheless, the definition of this link varies depending on the probability of the upconversion processes compared to the probability of the relaxation of each level to populate a lower-lying energy level (non-radiative multiphonon relaxation).[29] In the simplest of cases in which the relaxation to a lower level accounts for a much higher probability than upconversion, the slope is normally equal to *n*. In the case of UCNPs based on crystalline hosts with low phonon energies (such as fluorides), the multiphonon relaxation is not as probable as in other matrices and as a result, upconversion emissions are intense. Thus, the so-called "saturation regime" can be easily reached in which the upconversion probability is high enough to modify the previous statement. In these cases, the plot is no longer a straight line and *m* becomes lower than *n*, as is the case with our materials. For these reasons, the slope, *m*, has been calculated in each case considering only the lower power data, where saturation has a weaker effect and the relationship is closer to a straight line.

The values obtained demonstrate a strong influence of upconversion even for the lower excitation powers considered in the experiment. Moreover, they confirm the step-like upconversion process, since higher excited states account for larger *m* values. The intensity dependence on excitation power has been analyzed at two different temperatures, 10 ^{o}C and 60 ^{o}C (A and B in Figure 3, respectively). As it can be seen, the degree of saturation is lower at higher temperature, since in this case the obtained values are closer to the expected ones (the expected values are, 2 for $^{3}H_4$, 3 for $^{1}G_4$, 4 for $^{1}D_2$ and 5 for $^{1}I_6$).[30] This effect is easy to understand bearing in mind that high temperatures favor stimulated multiphonon emissions.[31] Therefore, the effect of the increased multiphonon relaxation rate at higher temperatures can be considered as detrimental for the upconverted emission intensities, since it favors a non-radiative relaxation route.

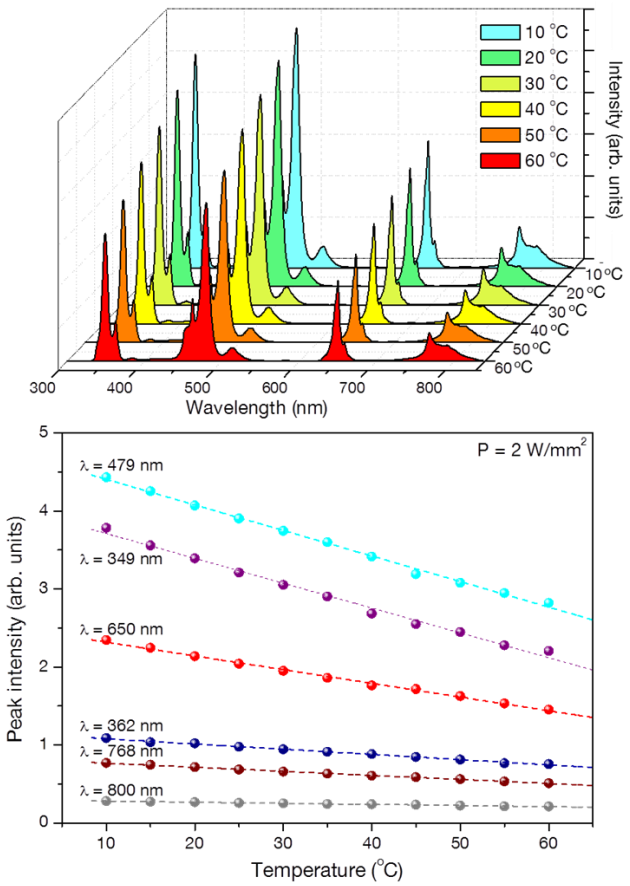

Figure 4. Temperature dependence of the emission bands of SrF_2:Tm^{3+}, Yb^{3+} UCNPs in a colloidal dispersion in D_2O. The dashed lines in the left graph have been added to guide eye.

To investigate the correlation between the temperature and upconversion emission intensities, the upconversion spectrum for the SrF_2:Tm^{3+}, Yb^{3+} UCNPs in a D_2O colloidal dispersion was recorded at different temperatures ranging between 10 ^{o}C and 60 ^{o}C. In Figure 4 the full spectra and the peak intensities of the main emissions are plotted versus temperature. It can be observed that the intensity of every emission band decreased when the temperature was increased. This decrease was calculated to be roughly 40% of the initial emission after increasing the temperature by 50 ^{o}C. This was the case for all the emissions analyzed excluding, however, the NIR emission from the $^{3}H_4$ level and the UV emission attributed to the $^{1}D_2$ level at 362 nm, which were observed to have a weaker decrease of around 25% and 30%, respectively, of the intensity for the same temperature range. These differences can be related to the different energy gaps to be bridged through multiphonon processes and the different excitation paths in which the states are populated. The higher phonon density linked to higher temperatures, apart from increasing multiphonon relaxations, can favor phonon-assisted energy transfer processes as well. Therefore, one effect might be partially compensated by the other. This particularly plays a role in the case of $^{1}D_2$ population routes, which as discussed above, are dependent on the strongly non-resonant Yb^{3+} to Tm^{3+} energy transfer as well as additional Tm^{3+} to Tm^{3+} cross-relaxation mechanisms.

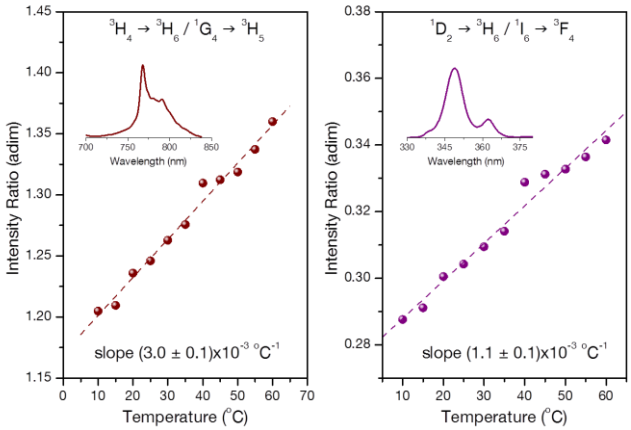

Figure 5. Dependence with temperature of two intensity ratios: one in the NIR ($^{3}H_4 \rightarrow {}^{3}H_6$ / $^{1}G_4 \rightarrow {}^{3}H_5$) at around 800 nm; and one in the UV ($^{1}D_2 \rightarrow {}^{3}H_6$ / $^{1}I_6 \rightarrow {}^{3}F_4$) at around 350 nm). The insets show the corresponding spectral range. The dashed lines are the linear fit of the experimental data. The corresponding slopes are also given in the graph.

It is worth mentioning that a possible use of the present UCNPs for biomedical applications would be in the physiological temperature range, between 35 and 40 ^{o}C. In this range, only a 1.6 % decrease of the emission intensity is observed for most of the visible and UV emission bands (a 1.2 % for $^{1}D_2$ state emissions). However, each emission band varies with a slightly different ratio as shown in Figure 4. The knowledge of these variations allows us to define the intensity ratios that will account for larger thermal sensitivities, which can be eventually applied for nanothermometry. For this purpose, the emission intensity of one single emission line could be used as well as a thermal probe (using Figure 4 as calibration curve), yet the recorded intensity would be dependent not only on temperature, but also on the local concentration of nanoparticles, which is a parameter hardly controlled in real experiments. This fact makes intensity ratios preferable, even more if the two emission peaks selected are close in wavelength and thus almost equally affected by absorption and scattering in the media. Following these ideas, here we define two ratios (Figure 5), one in the UV range around 350 nm ($^{1}D_2 \rightarrow {}^{3}H_6$ / $^{1}I_6 \rightarrow {}^{3}F_4$), and one in the NIR around 800 nm, where the transparency of biological samples is higher ($^{3}H_4 \rightarrow {}^{3}H_6$ / $^{1}G_4 \rightarrow {}^{3}H_5$). The ratio in the UV instead is not expected to be applied in situations where high penetration depth is required, since biological tissues strongly absorb these wavelengths. However,

it is characterized by multiphotonic (4 and 5 photons) processes and thus, is expected to offer a good spatial resolution, which can be a great advantage for thermometry applications on nanostructured surfaces. The calibration curves of these two ratios following 2 W/mm^2 excitation light are given in Figure 5. From the figure it is clear that the sensitivity of the NIR option, i.e. the slope of the linear fit, is three times larger than the UV one.

Up to this point, all the experiments were carried out in colloidal dispersion of UCNPs in D_2O as a solvent. In order to study the effect of the higher energy phonons from the solvent molecules that are in contact with the UCNP surface on the upconversion emission properties, we investigated colloidal dispersions with different D_2O/H_2O ratios and constant concentration of nanoparticles (1 wt%). This investigation is particularly important since using H_2O as a solvent, the emission intensity is expected to decrease due to the increased multiphonon relaxation, but this is the required environment in biological applications. The upconversion emission spectra were recorded in the different dispersions at a constant temperature of 35 ^oC, and the results were analyzed considering the peak intensity of each emission band. The obtained data are plotted in Figure 6A. We observed that the presence of H_2O reduces all the emission intensities, and this effect is different for the various emission bands.

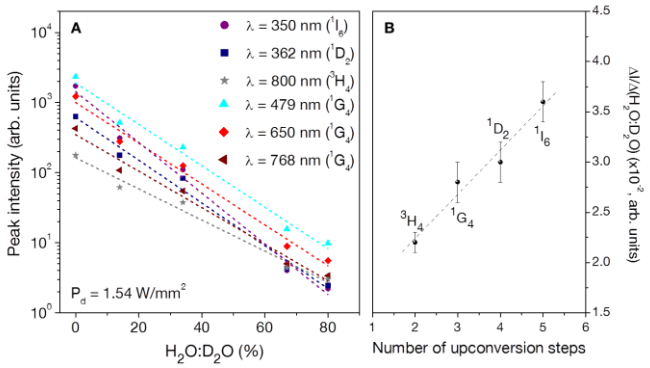

Figure 6. (A) Variation of the emission band intensities of SrF_2:Tm^{3+}, Yb^{3+} colloidal dispersions as a function of the solvent (mix of D_2O and H_2O). The dotted lines are linear fits of the experimental data. The slopes obtained from the linear fits are plotted in (B) versus the number of up-conversion steps required to populate each Tm^{3+} state.

The data can be fitted to a straight line (dotted lines in the figure) where the slope can provide an indication on the strength of the effect for each emission. In Figure 6B the obtained slopes (and their related standard error) are plotted versus the number of upconversion steps required to populate the specific state (see the scheme in Figure 2). In this way, it becomes evident that the upconversion processes requiring a larger number of excitation steps are affected by the presence of H_2O to a larger extent. These results are consistent with our hypothesis, since quenching from water phonons takes place at higher energies (in the NIR) and modifies the upconversion probabilities from the basis of the whole process; therefore, its effect is accumulated after each sequential step. Moreover, water is not completely transparent to the excitation wavelength,[8] and thus, Yb^{3+} ions will be less excited when the water content is higher. This would also affect upconversion processes from the very beginning of the mechanism and therefore, the effect can be accumulated along the individual steps as well. Finally, it is interesting to note that while the most intense UV emission band is due to the $^1I_6 \rightarrow {}^3F_4$ transition (around 290 nm) when pure D_2O is used as solvent, the band at 362 nm attributed to the $^1D_2 \rightarrow {}^3H_6$ transition becomes more important in aqueous media.

Conclusions

In this paper 9 nm diameter SrF_2:Tm^{3+}, Yb^{3+} UCNPs have been synthesized following a hydrothermal route and their emission properties after 980 nm excitation have been discussed. Strong UV emissions bands, associated to transitions from the $^1D_2$ and $^1I_6$ Tm^{3+} excited states, are observed. Their intensities have been shown to be dependent on temperature due to the increased multiphonon relaxation rates at higher temperatures. The thermal effect, though, has been observed to be weaker for $^1D_2$ emissions, most probably due to the effect of temperature on the excitation routes. The quenching effect of H_2O has been studied as well, and it is shown to be more important for higher Tm^{3+} excited states when they are excited through upconversion. It is interesting to underline that the emission of the $^1D_2$ state is less affected from H_2O quenching than the $^1I_6$ state. For these reasons, although the $^1I_6$ ultraviolet emission intensity is generally stronger, $^1D_2$ ultraviolet emissions could be considered for possible UV generation upon NIR excitation in which the quenching effect of H_2O is important.

Acknowledgements

Dr. M. Quintanilla would like to thank Fundación Ramón Areces for financial support through their granting program for Life and Matter Sciences. Prof. F. Vetrone is grateful for financial support from the Natural Sciences and Engineering Research Council (NSERC) of Canada, the Canadian Institute for Photonic Innovations (CIPI) and the Fonds de recherche du Québec – Nature et technologies (FRQNT) for supporting his research. Fondazione Cariverona (Verona, Italy) is gratefully acknowledged by Prof. A. Speghini for financial support in the frame of the project "Verona Nanomedicine Initiative".

Notes and references

[a] Institut National de la Recherche Scientifique - Énergie, Matériaux et Télécommunications (INRS - EMT), Université du Québec, 1650 Boul. Lionel-Boulet, Varennes, QC, J3X 1S2 (Canada).
Email : vetrone@emt.inrs.ca
[b] Dipartimento di Biotecnologie, Università di Verona and INSTM, UdR Verona, Strada Le Grazie 15, I-37314 Verona (Italy).
Email : adolfo.speghini@univr.it
[c] Centre for Self-Assembled Chemical Structures, McGill University, Montreal, QC, H3A 2K6 (Canada).

References

1. G. Chen, H. Qiu, P. N. Prasad and X. Chen, *Chem. Rev.*, 2014, **114**, 5161-5214.
2. S. Thompson, A. C. Self and C. H. Self, *Drug Disc. Today Targets*, 2010, **15**, 468-473.
3. S. W. Pridgeon, R. Heer, G. A. Taylor, D. R. Newell, K. O'Toole, M. Robinson, Y.-Z. Xu, P. Karran and V. Boddy, *Br. J. Cancer*, 2011, **104**, 1869-1876.

4. O. Reelfs, P. Karran and A. R. Young, *Photochem. Photobiol.*, 2012, **11**, 148-154.
5. D. M. Blake, P.-C. Maness, Z. Huang, E. J. Wolfrum, J. Huang and W. A. Jacoby, *Sep. Purif. Rev.*, 1999, **28**, 1 - 50.
6. W. P. Qin, D. S. Zhang, D. Zhao, L. L. Wang and K. Z. Zheng, *Chem. Commun.*, 2010, **46**, 2304-2306.
7. X. Y. Guo, W. Y. Song, C. F. Chen, W. H. Di and W. P. Qin, *PCCP*, 2013, **15**, 14681-14688.
8. A. M. Smith, M. C. Mancini and S. Nie, *Nat. Nanotechnol.*, 2009, **4**, 710.
9. L. M. Maestro, J. E. Ramirez-Hernandez, N. Bogdan, J. A. Capobianco, F. Vetrone, J. G. Sole and D. Jaque, *Nanoscale*, 2012, **4**, 298-302.
10. F. Wang and X. Liu, *Chem. Soc. Rev.*, 2009, **38**, 976-989.
11. Y. S. Liu, D. T. Tu, H. M. Zhu and X. Y. Chen, *Chem. Soc. Rev.*, 2013, **42**, 6924-6958.
12. F. Auzel, *Chem. Rev.*, 2004, **104**, 139-173.
13. G. Wang, W. P. Qin, L. L. Wang, G. D. Wei, P. Zhu, D. Zhang and F. Ding, *J. Rare Earth*, 2009, **27**, 330-333.
14. F. Shi and Y. Zhao, *J. Mater. Chem. C*, 2014, **2**, 2198-2203.
15. H. Qiu, G. Chen, R. Fan, L. Yang, C. Liu, S. Hao, M. J. Sailor, H. Agren, C. Yang and P. N. Prasad, *Nanoscale*, 2014, **6**, 753-757.
16. V. Mahalingam, F. Vetrone, R. Naccache, A. Speghini and J. A. Capobianco, *Adv. Mater.*, 2009, **21**, 4025-4028.
17. A. Bensalah, M. Ito, Y. Guyot, C. Goutaudier, A. Jouini, A. Brenier, H. Sato, T. Fukuda and G. Boulon, *J. Lumin.*, 2007, **122**, 444-446.
18. A. Bensalah, M. Mortier, G. Patriarche, P. Gredin and D. Vivien, *J. Solid State Chem.*, 2006, **179**, 2636-2644.
19. P. Camy, J. L. Doualan, A. Benayad, M. von Edlinger, V. Menard and R. Moncorge, *Appl. Phys. B*, 2007, **89**, 539-542.
20. F. Druon, S. Ricaud, D. N. Papadopoulos, A. Pellegrina, P. Camy, J. L. Doualan, R. Moncorge, A. Courjaud, E. Mottay and P. Georges, *Opt. Mater. Express*, 2011, **1**, 489-502.
21. W. Hayes, *Crystals with the Fluorite Structure: Electronic, Vibrational and Defect Properties*, Oxford University Press, Oxford, UK, 1974.
22. M. M. Lage, A. Righi, F. M. Matinaga, J. Y. Gesland and R. L. Moreira, *J. Phys.: Condens. Matter*, 2004, **16**, 3207.
23. J. Suyver, J. Grimm, M. K. van Veen, D. Biner, K. W. Krämer and H. U. Güdel, *J. Lumin.*, 2006, **117**, 1-12.
24. M. Pedroni, F. Piccinelli, T. Passuello, S. Polizzi, J. Ueda, P. Haro-Gonzalez, L. M. Maestro, D. Jaque, J. Garcia-Sole, M. Bettinelli and A. Speghini, *Cryst. Growth Des.*, 2013, **13**, 4906-4913.
25. R. P. Singh, Y. D. Yeboah, E. R. Pambid and P. Debayle, *J. Chem. Eng. Data*, 1991, **36**, 52-54.
26. M. Pedroni, F. Piccinelli, T. Passuello, S. Polizzi, J. Ueda, P. Haro-Gonzalez, L. M. Maestro, D. Jaque, J. Garcia-Sole, M. Bettinelli and A. Speghini, *Crystal Growth & Design*, 2013, **13**, 4906-4913.
27. H. Zhang, Y. J. Li, Y. C. Lin, Y. Huang and X. F. Duan, *Nanoscale*, 2011, **3**, 963-966.
28. G. F. Wang, W. P. Qin, L. L. Wang, G. D. Wei, P. Zhu and R. J. Kim, *Opt. Express*, 2008, **16**, 11907.
29. M. Pollnau, D. R. Gamelin, S. R. Lüthi and H. U. Güdel, *Phys. Rev. B: Condens. Matter*, 2000, **61**, 3337-3346.
30. C. Cao, W. Qin, J. Zhang, Y. Wang, P. Zhu, G. Wang, G. Wei, L. Wang and L. Jin, *J. Fluorine Chem.*, 2008, **129**, 204-209.
31. M. J. Weber, *Phys. Rev. B: Condens. Matter*, 1973, **8**, 54-64.

Table of Contents

Ultrasmall and water dispersible $SrF_2:Tm^{3+}$, Yb^{3+} upconverting nanoparticles show intense ultraviolet emissions after 980 nm excitation.